PNAS RESEARCH ARTICLE | BIOCHEMISTRY CHEMISTRY

Siglec-15/sialic acid axis as a central glyco-immune checkpoint in breast cancer bone metastasis

Yixian Wang[a,1], Zhan Xu[b,1], Kuan-Lin Wu[a], Liqun Yu[b], Chenhang Wang[a], Haoxue Ding[a], Yang Gao[b], Han Sun[a], Yi-Hsuan Wu[b], Meng Xia[a], Yuda Chen[a], and Han Xiao[a,c,d,2]

Edited by Carolyn Bertozzi, Stanford University, Stanford, CA; received July 27, 2023; accepted December 6, 2023

Immunotherapy is a promising approach for treating metastatic breast cancer (MBC), offering new possibilities for therapy. While checkpoint inhibitors have shown great progress in the treatment of metastatic breast cancer, their effectiveness in patients with bone metastases has been disappointing. This lack of efficacy seems to be specific to the bone environment, which exhibits immunosuppressive features. In this study, we elucidate the multiple roles of the sialic acid–binding Ig-like lectin (Siglec)-15/sialic acid glyco-immune checkpoint axis in the bone metastatic niche and explore potential therapeutic strategies targeting this glyco-immune checkpoint. Our research reveals that elevated levels of Siglec-15 in the bone metastatic niche can promote tumor-induced osteoclastogenesis as well as suppress antigen-specific T cell responses. Next, we demonstrate that antibody blockade of the Siglec-15/sialic acid glyco-immune checkpoint axis can act as a potential treatment for breast cancer bone metastasis. By targeting this pathway, we not only aim to treat bone metastasis but also inhibit the spread of metastatic cancer cells from bone lesions to other organs.

glycocalyx | sialic acid | Siglec | bone | glycobiology

Significance

The glycocalyx, a network of glycolipids and glycoproteins on cell surfaces, plays a pivotal role in immune modulation. Hypersialylated glycans have been identified as an immune suppressive marker, are exploited by tumors to evade immune recognition, and lead to suboptimal effectiveness of immune checkpoint blockade therapy in bone metastases. Here, we elaborated on the important roles of Siglec-15 in breast cancer bone metastases and bone microenvironment. We reported that Siglec-15/sialic acid axis represents as a glycoimmune checkpoint and modulator of tumor-induced osteoclastogenesis for bone cancers, and demonstrated that targeting the Siglec-15/sialic acid axis by anti-Siglec-15 antibody represents a promising approach for patients with breast cancer bone metastases.

The bone is a common site for breast cancer metastasis, affecting more than 70% of patients with metastatic breast cancer (1, 2). This can lead to skeletal-related events like osteoporosis, fractures, and hypercalcemia, resulting in a decreased quality of life and increased mortality rates (3–6). Interestingly, recent genomic analyses have revealed that the bone is not the final destination for metastasis. In over two-thirds of cases, bone metastases continue to spread to other organs through a process called "metastasis-to-metastasis seeding", ultimately contributing to patient mortality (1, 7–9). As a new class of cancer treatments, immune checkpoint inhibitors such as Atezolizumab, Pembrolizumab, Ipilimumab, Relatlimab, and others have emerged as promising options (10, 11). However, only a small subset of patients with bone cancer benefits from these novel treatments (12).

The glycocalyx, a sugar-rich coating present on the surface of tumor and immune cells, is exploited by cancer cells to evade recognition by immune cells and suppress anti-tumor immune responses. One frequently observed phenomenon in cancer is hypersialylation, where sialic acid–rich glycans play a role. Similar to PD-L1, which leads to T cell exhaustion, sialylated glycans enable tumors to escape immune surveillance by engaging recently discovered sialic acid–binding Ig-like lectin (Siglec) immunoreceptors found on various types of leukocytes (13–19). Siglecs are transmembrane receptors that bind to sialic acid and are expressed by immune, hemopoietic, and nerve cell (15). In humans, there are 14 Siglec receptors, many of which possess a cytosolic immunoreceptor tyrosine-based inhibitory motif (ITIM) or immunoreceptor tyrosine-based activation motif (ITAM) that regulates immune cell activities. One prominent Siglec, Siglec-2 (CD22), is involved in cell adhesion and negatively regulates the B cell receptor (20–27). Due to its exclusive expression on B cells, Siglec-2 is an attractive target for treating autoimmune diseases and B cell malignancies (27–29). Several studies suggest that hypersialylation of cancer cells contributes to immune evasion from macrophages, natural killer (NK) cells, neutrophils, and T cells. A study demonstrated that human Siglec-9 or mouse Siglec-E induces macrophages to adopt an immunosuppressive tumor-associated macrophage (TAM) phenotype, inhibiting the endogenous anti-tumor immune response and promoting tumor progression and metastasis. Novel antibodies that target Siglec-9 can significantly reduce ovarian tumor growth in a humanized mouse model (30). Dense clusters of sialylated glycans on the cell surface can recruit NK cell-associated Siglec-7/9 to the immune synapse, thereby suppressing the immune response. An antibody–sialidase conjugate, known as a Glyco-Immune Checkpoint inhibitor, enables the blocking of Siglec/sialic acid interactions by selectively removing sialic acid from the tumor cell glycocalyx, both in laboratory experiments and animal models (31–35). These tumor glycosignatures strongly correlate

Author contributions: Y.W., Z.X., K.-L.W., and H.X. designed research; Y.W., Z.X., K.-L.W., L.Y., C.W., H.D., Y.G., H.S., Y.-H.W., M.X., and Y.C. performed research; Y.W., Z.X., K.-L.W., C.W., and H.X. contributed new reagents/analytic tools; Y.W., Z.X., K.-L.W., L.Y., C.W., H.D., Y.G., H.S., Y.-H.W., M.X., Y.C., and H.X. analyzed data; and Y.W., Z.X., K.-L.W., L.Y., C.W., H.D., Y.G., H.S., Y.-H.W., M.X., Y.C., and H.X. wrote the paper.

The authors declare no competing interest.

This article is a PNAS Direct Submission.

[1]Y.W. and Z.X. contributed equally to this work.

[2]To whom correspondence may be addressed. Email: han.xiao@rice.edu.

This article contains supporting information online at https://www.pnas.org/lookup/suppl/doi:10.1073/pnas.2312929121/-/DCSupplemental.

Published January 22, 2024.

with a poor prognosis, but their functional contribution and targeted therapeutic strategies have remained unclear, particularly for bone metastatic cancers.

Notably, Siglec-15, a member of the Siglec family proteins, is primarily expressed on a subset of myeloid cells under normal conditions but is upregulated on human cancer cells and tumor-infiltrating myeloid/macrophage cells (36–39). Recent studies have identified Siglec-15 as an immune regulator. Elevated levels of Siglec-15 on tumors and tumor-infiltrating myeloid cells have been shown to suppress antigen-specific T cell proliferation and function both in vitro and in vivo (Fig. 1*A*) (38, 40). In a mouse melanoma model (using the B16-GMCSF cell line that overexpresses GM-CSF, a cytokine involved in recruiting myeloid cells to tumors), specific blockade of Siglec-15 enhanced anti-tumor immunity in the tumor microenvironment (TME) and inhibited tumor growth (38). Furthermore, Siglec-15 is also known to regulate osteoclast differentiation and function. Osteoclast differentiation is primarily driven by the receptor activator of NF-κB (RANK) signaling pathway, which is initiated by the binding of the RANK ligand (RANKL) (41). Upon interaction with sialic acids, Siglec-15 on osteoclast precursor cells associates with DNAX-activating protein of 12 kDa (DAP12), which contains an ITAM domain (42–47). This association between Siglec-15 and DAP12 induces downstream signal transduction of RANK, leading to osteoclast maturation. Blocking Siglec-15 can suppress osteoclast differentiation, and Siglec-15 knockout mice have shown mild osteopetrosis and reduced urinary deoxypyridinoline levels. Hence, the significance of Siglec-15 in osteoclastogenesis suggests that it may play an essential role in bone metastasis since the increased differentiation and activity of osteoclasts are crucial for the formation of the "vicious cycle" of osteolytic breast cancer bone metastases. The vicious cycle between bone destruction and tumor growth is driven by paracrine crosstalk among cancer cells, osteoblasts, and osteoclasts. Specifically, cancer cells secrete molecules such as parathyroid hormone–related protein (PTHrP) that act on osteoblasts to modulate the expression of genes, including RANKL and osteoprotegerin (OPG). Increased levels of RANKL can lead to osteoclast maturation, resulting in bone matrix resorption and the release of TGF-β and other growth factors. These factors stimulate osteoblasts as well as bone tumor cells, further amplifying the vicious cycle. These findings suggest that Siglec-15 may serve as a central glyco-immune checkpoint axis for osteolytic bone metastasis.

In our study, we found elevated levels of Siglec-15 in both tumor-infiltrating macrophage cells and osteoclasts within the bone metastatic niche. The enhanced Siglec-15 level in the bone metastatic niche significantly promotes tumor-induced osteoclastogenesis and inhibits T cell activities in bone metastatic models. Moreover, the differentiated osteoclasts in the bone metastatic niche effectively suppress T cells by interacting with Siglec-15. By employing several syngeneic breast cancer bone metastasis models, we demonstrated that targeted blockade of Siglec-15 within the bone metastatic niche effectively impedes the growth of bone metastases and prevents the seeding of additional metastases to other organs from bone lesions.

Results

Overexpression of Siglec-15 in the Bone Metastatic Niche. According to data from The Cancer Genome Atlas (TCGA) program, Siglec-15 is found to be overexpressed in various cancer types, such as breast cancer, kidney cancer, liver cancer, lung cancer, esophageal cancer, pancreatic adenocarcinoma, and others. The overexpression of Siglec-15 is associated with a poor prognosis and the presence of an immune suppressive microenvironment. Recent studies have identified Siglec-15 as

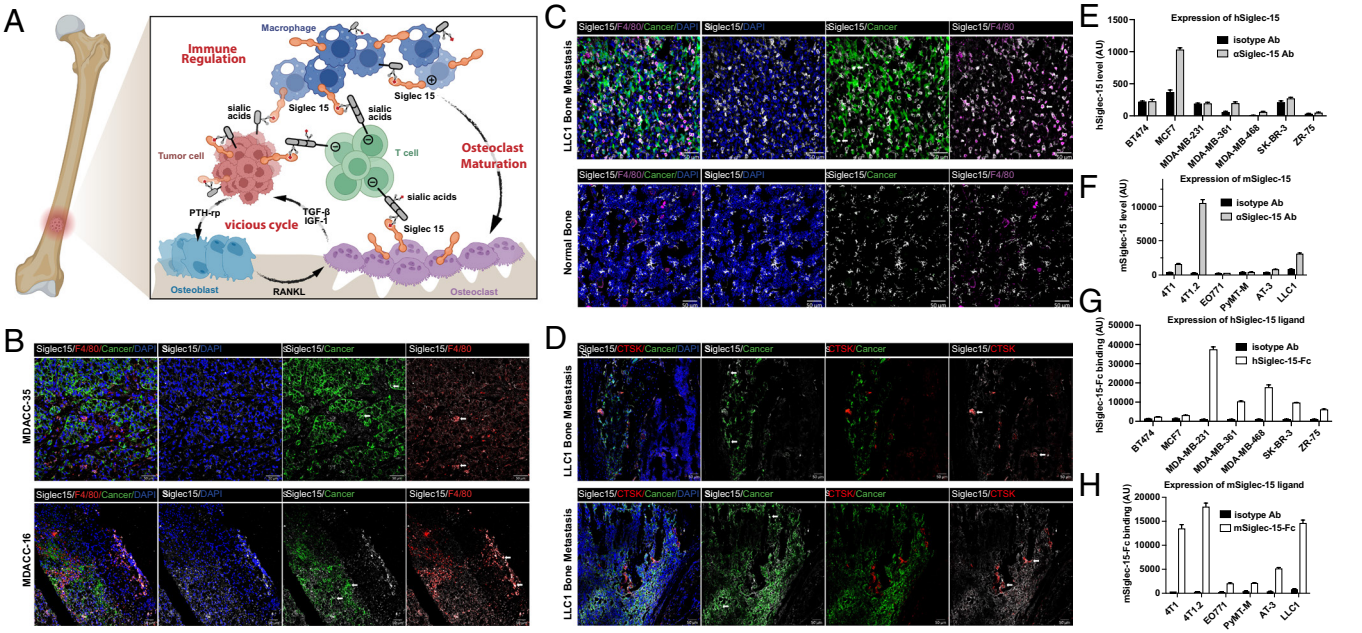

Fig. 1. Siglec-15 is abundant in bone metastatic niche. (*A*) Schematic of hypothesized Siglec-15 mechanism: Siglec-15 involves in the crosstalk of metastatic bone tumors, osteoclasts, TAM, and T cells. Siglec-15 suppresses T cell function, induces osteoclast maturation, and promotes the vicious cycle. (*B*) Representative immunofluorescence staining of patient samples from MD Anderson Cancer Center. Macrophage marker F4/80 (red), cancer (green), Siglec-15 (white), and nuclei (blue). Representative Siglec-15 expressing cells (white arrow). (Scale bar, 50 μm.) (*C*) Representative immunofluorescence staining of metastatic bone niche compared with normal bone from an LLC1 bone metastases–bearing mouse. Macrophage marker F4/80 (magenta), cancer (green), Siglec-15 (white), and nuclei (blue). Representative Siglec-15 expressing cells (white arrow). (Scale bar, 50 μm.) (*D*) Representative immunofluorescence staining of metastatic bone niche from an LLC1 bone metastases–bearing mouse. Osteoclast marker cathepsin K (red), cancer (green), Siglec-15 (white), and nuclei (blue). (Scale bar, 50 μm.) (*E* and *F*) Expression levels of the Siglec-15 receptor on common human and mouse cell lines. (*G* and *H*) Expression levels of Siglec-15 ligands on common human and mouse cell lines.

an immune regulator, capable of suppressing antigen-specific T cell proliferation and function both in vitro and in vivo when present in high levels on tumors and tumor-infiltrating myeloid cells. To gain a deeper understanding of the role of Siglec-15 in the bone tumor microenvironment, the expression of Siglec-15 was studied in both clinical patient tumor samples and pre-clinical mouse models. First, we examined the expression of Siglec-15 in tumor samples resected from patients with bone metastatic cancers using immunofluorescence microscopy. Consistent with previous findings, Siglec-15 was found to be expressed on both cancer cells and tumor-infiltrating macrophages in the bone metastatic niches (Fig. 1*B* and *SI Appendix*, Figs. S1 and S2).

Furthermore, the expression of Siglec-15 was evaluated in the bone metastatic niches of a mouse model of bone metastasis. To establish a mouse model with bone metastasis, GFP-labeled LLC1 cells were injected into C57BL/6 mice via the intra-iliac artery (IIA) injection. After approximately 3 wk, the tumor-bearing bones were collected and examined under immunofluorescence microscopy. Similar to the observations in patient samples, Siglec-15 expressions on both cancer and macrophage cells were validated in our bone metastatic mouse model, what's more, a significant elevation of Siglec-15 was observed in the tumor-surrounding area compared to the distal normal bone tissue (Fig. 1*C* and *SI Appendix*, Figs. S3–S5). The aforementioned results indicate that Siglec-15 is present in various cell types within the tumor microenvironment in the bone, including macrophages. Based on previous research findings, it has been established that Siglec-15 plays a crucial role in the process of osteoclastogenesis. Furthermore, it has been observed that both osteoclasts and macrophages share a common origin, indicating a potential link between the two cell types. Indeed, an increase in Siglec-15 levels was also detected in the Ctsk-expressing osteoclasts neighboring bone metastatic tumor (Fig. 1*D*), suggesting that the upregulation of Siglec-15 on osteoclasts may also contribute to the immune suppressive microenvironment in these niches.

We conducted further investigations to examine the expression of Siglec-15 in a panel of mouse and human breast cancer cell lines using an anti-Siglec-15 antibody (Clone: 5G12) (*SI Appendix*, Figs. S6 and S7). Through flow cytometry analysis, we detected high expression levels of Siglec-15 on several mouse and human cell lines (Fig. 1*E* and *F* and *SI Appendix*, Figs. S8 and S9). In addition to assessing Siglec-15 expression, we also evaluated the expression levels of Siglec-15 ligands using recombinant chimeras of Siglec-15 fused to the IgG1 Fc domain. Previous studies suggest that the Siglec-15 ligands on cancer cells can engage Siglec-15 on macrophages, increasing the production level of immunosuppressive factor TGF-β (39, 48). We observed high expression levels of Siglec-15 ligands on most of the tested cell lines, consistent with previously reported findings (Fig. 1*G* and *H* and *SI Appendix*, Figs. S10–S12). To verify whether these ligands are sialic acid–containing ligands, we subjected the cell lines to sialidase treatment. The enzymatic removal of sialic acid from different mouse and human cell lines resulted in a significant decrease in Siglec-15 binding (*SI Appendix*, Fig. S13). It is worth noting that the expression level of Siglec-15 is relatively high in 4T1.2, 4T1, LLC1, and HCC1954 cells, which is consistent with their increased metastatic capability. 4T1.2, a single-cell clone of 4T1, exhibits a higher propensity for spontaneous bone metastasis, leading to fractures and/or hind limb paralysis. This observation aligns with the significantly elevated Siglec-15 expression level in 4T1.2 compared to its parental cell line, 4T1.

Inhibition of Tumor Growth in an Ex Vivo Bone Metastasis Model through Siglec-15 Blockade. To investigate the impact of blocking the interaction between Siglec-15 and Siglec-15 ligands on metastatic bone tumors, we utilized a previously reported ex vivo bone metastasis model known as the bone-in-culture array (BICA) (49, 50). The BICA model replicates the interactions between cancer cells and bone in both the pre-osteolytic and osteolytic phases by fragmenting mouse bones and incubating them with cancer cells (Fig. 2*A*) and serves as a valuable pre-clinical platform, bridging the gap between in vitro and in vivo models, and facilitating mechanistic and pharmacological studies of bone metastasis.

Tumor-free bone fragments containing bone marrow were collected and arranged in low-attachment plates for BICA experiments. EO771 cells, labeled with luciferase and GFP, were introduced to the cultures, along with varying concentrations of 5G12. Following incubation, cancer cells were imaged using bioluminescence or immunofluorescence microscopy. As shown in Fig. 2 *B* and *C*, treatment with Siglec-15 significantly enhanced the killing response against EO771 cells across various antibody concentrations in BICA. Notably, at a concentration of 10 μg/mL, the anti-Siglec-15 antibody achieved over 50% inhibition of tumor growth within a 7-d period in the BICA model (Fig. 2 *B* and *C*). Additionally, after 7 d, the bone fragments were examined using fluorescence microscopy. Consistent with the bioluminescence signal, treatment with 10 μg/mL of the anti-Siglec-15 antibody led to a substantial reduction in EO771 cell growth, as evidenced by decreased GFP signal (Fig. 2*D* and *SI Appendix*, Fig. S14). Moreover, 4T1 cells, labeled with luciferase from ATCC, were also used in this BICA assay and treated with varying concentrations of 5G12 as a validation. A similar dose-dependent cell-killing effect against 4T1 cells was observed (*SI Appendix*, Fig. S15). Given the observed upregulation of Siglec-15 in mature osteoclast cells in mouse samples with bone metastasis, we also conducted staining of the bone fragments using anti-CTSK and anti-Siglec-15 antibodies. As depicted in Fig. 2*D*, treatment with the anti-Siglec-15 antibody resulted in a notable decrease in both CTSK and Siglec-15 staining, suggesting that blocking the Siglec-15/sialic acid axis may influence the differentiation and activity of osteoclasts in the bone metastatic niches.

Blockage of Siglec-15 Inhibits Differentiation and Maturation of Osteoclasts in Bone Metastatic Niche. To validate the role of Siglec-15 in osteoclastogenesis within the bone metastatic niche, we examined the effects of an anti-Siglec-15 blocking antibody, 5G12, on RANKL–induced osteoclast formation. As expected, RANKL stimulation led to the significant formation of tartrate-resistant acid phosphatase (TRAP)–positive multinucleated osteoclasts (Fig. 2 *E* and *F*). This observation was supported by the increased expression of key osteoclast markers, such as CstK, dendritic cell-specific transmembrane protein (DC-stamp), and osteoclast-associated receptor (Oscar) identified by mRNA expressions (Fig. 2 *G–I*). The upregulation of CstK, Oscar, and DC-stamp peaked 4 d after incubation with RANKL, indicating osteoclasts differentiation. However, treatment with anti-Siglec-15 antibody significantly inhibited osteoclast differentiation, as confirmed by both morphological analysis and RT-qPCR (Fig. 2 *E–I*). Complete inhibition of osteoclastogenesis was achieved with 30 μg/mL of the anti-Siglec-15 antibody, consistent with our RT-qPCR findings. These results are in line with a previous study that investigated the regulatory role of Siglec-15 in osteoclasts during the development of osteopetrosis. Furthermore, anti-Siglec-15 treatment significantly inhibited the upregulation of Siglec-15 during osteoclastogenesis following RANKL stimulation, consistent with our observations in the BICA assay (Fig. 2 *J*). The maximum inhibitory effect of Siglec-15 blockade against osteoclastogenesis was observed when

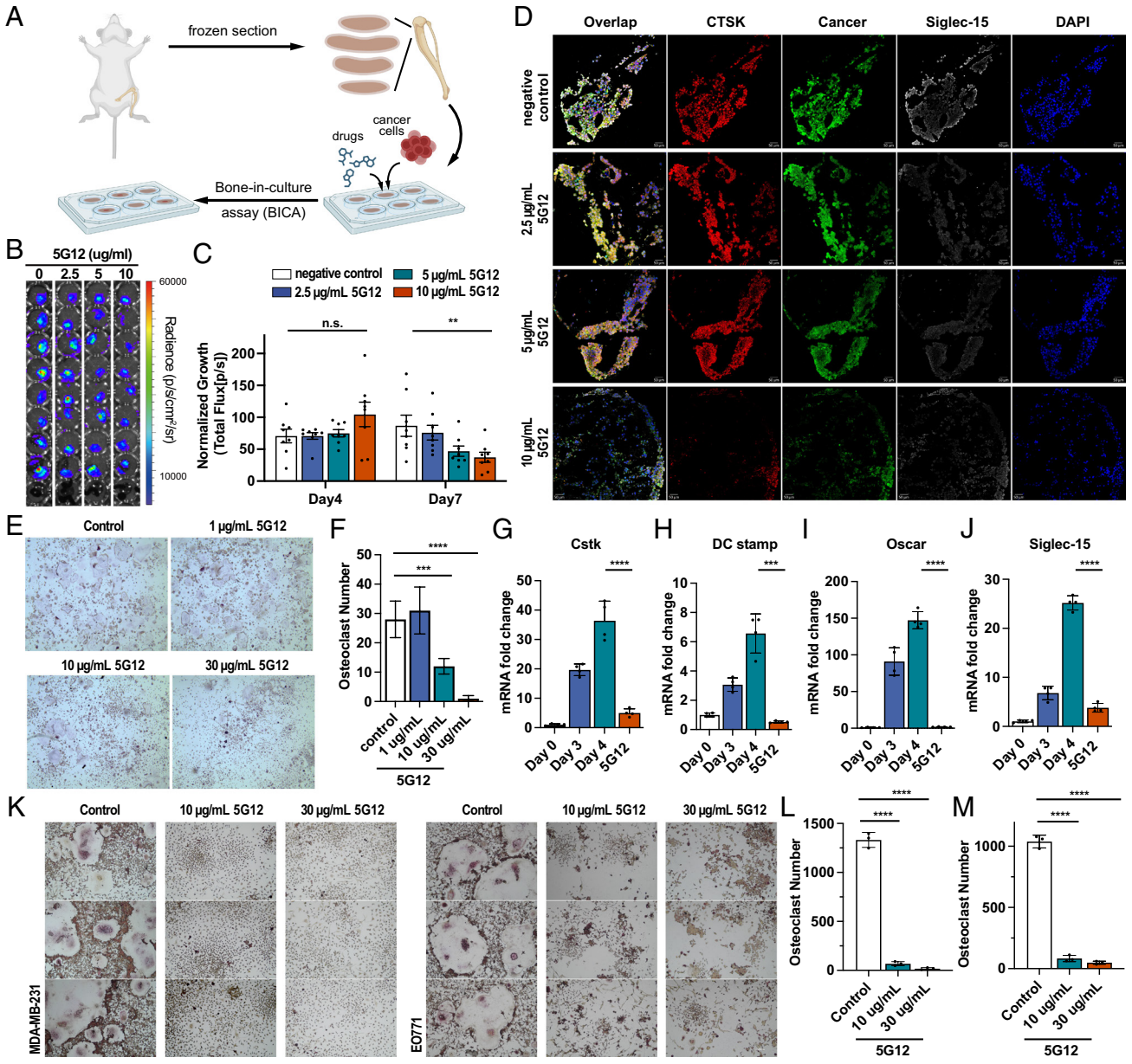

Fig. 2. Siglec-15 blockage inhibits differentiation and maturation of osteoclasts. (*A*) Schematic of BICA. (*B*) Representative pictures of EO771 BICA lesions at day 7 culture with different concentrations of 5G12. (*C*) Tumor lesion of BICA specimens with 5G12 treatment was quantified by bioluminescence total flux at different time points and normalized to day 0. Data are mean ± S.E.M. (n = 9 bone fragments per group). P values by two-way ANOVA. (*D*) Representative immunofluorescence staining of BICA specimens after 7-d culture. Osteoclast marker cathepsin K (red), cancer (green), Siglec-15 (white), and nuclei (blue). (Scale bar, 10 μm.) (*E*) Bright-field image of TRAP stained RANKL-induced RAW264.7 differentiation and maturation followed by treatment with the indicated doses, TRAP+ osteoclasts cells are shown in purple. (*F*) The TRAP-positive multinucleated (>3 nuclei) mature osteoclasts were counted. The P value was calculated by the unpaired t-test. (*G–J*) Expression levels of the osteoclast-specific marker gene, CstK (*G*), DC-stamp (*H*), Oscar (*I*), and Siglec-15 (*J*) on different time spots and 5G12 treatment. P values by two-way ANOVA. (*K*) Bright-field image of TRAP stained cancer cell–induced RAW264.7 differentiation and maturation followed by treatment with the indicated doses, mature osteoclasts (purple). (*L* and *M*) The TRAP-positive multinucleated (>3 nuclei) mature osteoclasts were counted for RAW264.7 coincubated with MDA-MB-231 (*L*) and EO771 (*M*) cells. The P value was calculated by the unpaired t-test. $^*P < 0.05$, $^{**}P < 0.01$, $^{***}P < 0.001$, and $^{****}P < 0.0001$.

the anti-Siglec-15 antibody was added during the early phase of RANKL treatment. In contrast, the suppressive effect was less pronounced when the anti-Siglec-15 antibody was added during the late stages, suggesting that the antibody primarily inhibits early osteoclast formation.

In the vicious cycle of osteolytic bone metastasis, tumor-secreted PTHrP modulates gene expression in osteoblasts, including RANKL and OPG, thereby stimulating osteoclast maturation and accelerating bone resorption. To further investigate the role of Siglec-15 in this vicious cycle, we employed a cancer-induced osteoclastogenesis assay. In the co-culture system, different ratios of RAW264.7 cells and tumor cells (MDA-MB-231 and EO771) were added to the plate, followed by the treatment with varying concentrations of an anti-Siglec-15 antibody. The addition of breast cancer cells significantly enhanced the osteoclastic bone resorption activity, while the blockade of Siglec-15 using the anti-Siglec-15 antibody resulted in significant inhibition of tumor cell-mediated osteoclastogenesis (Fig. 2 *K–M*). These findings demonstrate that the inhibition of Siglec-15 through the use of an anti-Siglec-15 antibody can effectively impede the differentiation and maturation of osteoclasts within the osteolytic bone metastatic niches.

Osteoclasts Inhibit T Cell Responses through the Siglec-15/Sialic Acid Interactions in the Bone Metastatic Microenvironment. A previous study suggested that Siglec-15, present on tumor-associated macrophages, can suppress T cell responses by interacting with the sialic acid ligands on the T cell surface. Thus, the high expression level of Siglec-15 on osteoclasts, which we observed in the bone metastatic niche, may also contribute to the immune suppressive microenvironment of bone metastasis by inhibiting T cell activities. To assess the T cell suppression of Siglec-15 on osteoclasts, we conducted co-incubation experiments with osteoclasts and CD3/CD28 activated $CD8^+$ T cells in the presence or absence of osteoclasts. As shown in Fig. 3 *A*–*D* and *SI Appendix*, Fig. S16, the incubation of T cells with osteoclasts dramatically decreased T cell numbers and led to a higher expression level of T cell exhaustion marker PD-1, TIM-3, and LAG-3. To demonstrate the involvement of Siglec-15 in this process, we employed a Siglec-15 blocking antibody. Blocking Siglec-15 alleviates the immunosuppressive effects of osteoclasts in a dose-dependent manner, thereby restoring $CD8^+$ T cell proliferation and reversing T cell exhaustion (Fig. 3 *A*–*D*). Besides blockage of direct interaction of osteoclasts and T cells by 5G12, we also studied the changes in cytokine release of osteoclasts after applying 5G12, since osteoclast is a paracrine cell. We compared cytokine levels in the supernatants of preosteoclasts, osteoclasts, and 5G12-treated osteoclasts. The result indicated that expression of TNF-α and IL-6 is significantly increased in the 5G12 treated group compared

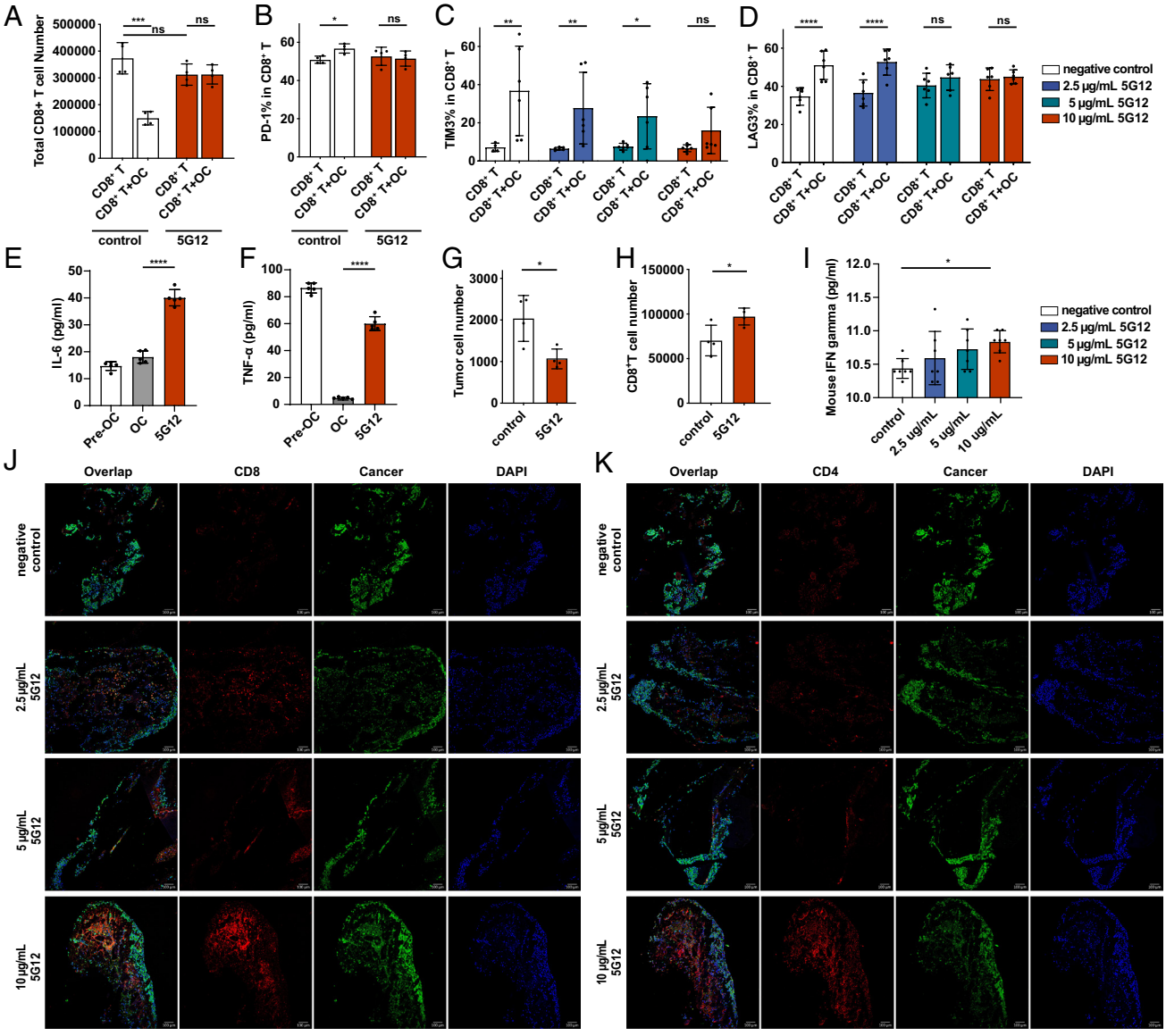

Fig. 3. 5G12 prevents osteoclast-mediated inhibition of T cells. (*A*) Flow cytometric quantification of $CD8^+$ T cells after co-cultured with osteoclasts with or without 5G12 treatment, $n = 4$ independent experiments. The *P* value was calculated by the paired *t*-test. (*B*) Flow cytometric quantification of the percentage of PD-1^+ CD-8^+ T cells in total $CD8^+$ T cells after co-cultured with osteoclasts with or without 5G12 treatment, $n = 4$ independent experiments. The *P* value was calculated by the paired *t*-test. (*C* and *D*) Flow cytometric quantification of the percentage of $TIM3^+$ and $LAG3^+$ CD-8^+ T cells in total $CD8^+$ T cells after co-cultured with osteoclasts with or without 5G12 treatment, respectively, $n = 6$ independent experiments. The *P* value was calculated by two-way ANOVA. (*E* and *F*) ELISAs of cytokine release of pre-osteoclasts, osteoclasts, and osteoclasts treated with 5G12, $n = 6$ independent experiments. The *P* value was calculated by the paired *t*-test. (*G*) tumor cell were counted in T cells, osteoclasts, and tumor cells co-culture with or without 5G12 treatment. (*H*) cytotoxic $CD8^+$ T cells count after co-culturing T cells, osteoclasts, and tumor cells with or without 5G12 treatment. The *P* value was calculated by the paired *t*-test. (*I*) Quantification of mouse IFN-γ in BICA culture medium at day 7. The *P* value was calculated by ordinary one-way ANOVA. (*J*) Representative immunofluorescence staining of BICA. $CD8^+$ T cell (red), cancer (green), and nuclei (blue). (Scale bar, 100 μm.) (*K*) Representative immunofluorescence staining of BICA. $CD4^+$ T cell (red), cancer (green), and nuclei (blue). $P > 0.05$ [not significant (n.s.)], $^*P < 0.05$, $^{**}P < 0.01$, $^{***}P < 0.001$, and $^{****}P < 0.0001$.

with osteoclasts (Fig. 3 *E* and *F*). Both cytokines promote T cell proliferation and activation, suggesting that 5G12 restores the T cell function through activating the paracrine function of macrophages. To further demonstrate that osteoclasts can inhibit T cell activities in the bone metastatic niche, we performed an in vitro ovalbumin (OVA)-specific cytotoxic $CD8^+$ T cell killing assay. By initially co-incubated osteoclasts, activated OT-I $CD8^+$ T cells, and EO771-OVA cancer cells, we found that blocking Siglec-15 significantly increased the number of cytotoxic $CD8^+$ T cells against OVA-expressing tumor cells. This, in turn, leads to a higher incidence of cancer cell death through cytotoxic T lymphocytes-mediated killing (Fig. 3 *G* and *H*). Since 5G12 was added to the experimental group, to make sure the cell-killing effect did not come from the 5G12 antibody itself, a cytotoxicity check was performed by incubating EO771 and MDA-MB-231 with different concentrations of 5G12, the result confirmed up to 50 μg/mL of 5G12, no obvious toxicity was observed (*SI Appendix*, Fig. S17). Subsequently, we employed BICA to evaluate the role of Siglec-15 blocking in inducing T cell responses in the bone metastatic niche. Through fluorescence imaging analysis of CD4 and CD8 T cell subsets, we observed increased tumor-infiltrating CD8 and CD4 T cells when higher concentrations of the anti-Siglec-15 antibody, 5G12, were present (Fig. 3 *J* and *K*). Furthermore, we also found that the IFN-γ secretion in the BICA supernatant increased in the 5G12-treated group (Fig. 3*I*), consistent with enhanced T cell proliferation and cytotoxicity. These findings indicate that mature osteoclasts expressing high levels of Siglec-15 can suppress IFN-γ production, leading to reduced proliferation and cytotoxicity of T cells. However, blocking the interaction between osteoclasts and T cells using a Siglec-15 antibody can restore T cell activities within the bone metastatic niche.

Siglec-15 Blocking Antibody Inhibited the Growth of Bone Metastasis in Murine Models. To investigate the potential of blocking the unique multifunctional glyco-immune checkpoint in the bone microenvironment to suppress osteolytic breast cancer bone metastasis, we evaluated the in vivo efficacy of an anti-Siglec-15 antibody in several syngeneic breast tumor models, including 4T1, EO771, and EMT-6. The 4T1 cell line, a triple-negative (ER, PR, and HER2 negative) murine cell line, is widely used as a metastatic breast cancer model in BALB/c mice. We injected 1×10^4 4T1 cells labeled with firefly luciferase into the right hind limb of BALB/c mice via para-tibial injection. Two days after injection, the mice were treated with the anti-Siglec-15 antibody through intraperitoneal injection. The anti-Siglec-15 antibody treatment exhibited remarkable efficacy, as nearly all animals responded positively to the therapy. Notably, most animals even achieved complete tumor regressions (CRs) after receiving the second treatment (Fig. 4 *A* and *B*). By the third treatment, all nine animals in the 5G12-treated group showed complete regression (Fig. 4 *A* and *B*). In contrast, the control group exhibited rapid tumor growth and reached the humane endpoint within 18 d. Moreover, the 5G12-treated group of mice experienced a 100% survival rate.

In contrast, the control group had a survival rate of only 11% (Fig. 4*C*). Treatment with the 5G12 antibodies was well tolerated, as no evident signs of toxicity were observed. There were no differences in body weight among the various treatment groups (Fig. 4*D*). At the end of the experiment, the tibiae from the tumor-bearing legs were harvested and subjected to micro-computed tomography (micro-CT) scanning. Encouragingly, the tibiae from the 5G12-treated mice exhibited greater bone volume (BV, Fig. 4 *E* and *F* and *SI Appendix*, Fig. S18), a higher bone volume/tissue volume ratio (BV/TV, Fig. 4 *E* and *G*), and thicker trabecular bone (Tb.Th, Fig. 4 *E* and *I* and *SI Appendix*, Fig. S18), while showing a smaller bone surface/bone volume ratio (BS/BV, Fig. 4 *E* and *H*) compared to those from the control group, indicating that 5G12 treatment significantly inhibited bone destruction during metastatic tumor growth. Histological analysis also supports that blocking of Siglec-15 prevents the massive invasion of tumor cells into the bone matrix and the adjacent tissue. Bone matrix is generally destroyed in bones with high tumor burden, whereas bones with less tumor burden in the 5G12-treated group exhibit intact bone matrix (Fig. 4*J*). Tartrate-resistant acid phosphatase (TRAP) staining of bone sections identified reduced numbers of osteoclasts (pink cells) in Fig. 4 *K* and *L*, indicating that osteogenesis is significantly inhibited by 5G12. To validate the therapeutic effect, human IgG1 was used as an isotype control antibody, similar results were obtained compared with the previous study (Fig. 4 *M*–*P*).

To demonstrate that anti-Siglec-15 treatment can be a general strategy for reversing the immunosuppressive microenvironment of the bone metastatic niche, we conducted experiments using two additional mouse models, EO771 and EMT-6. EO771 is a C57BL/6 cell line that functionally resembles the triple-negative subtype due to its truncated estrogen receptor (ER) without estrogen responses. We injected 1×10^5 EO771 cells labeled with firefly luciferase and GFP into the right hind limb of C57BL/6 J mice through para-tibial injection. As shown in Fig. 4 *Q* and *R*, mice treated with the anti-Siglec-15 antibody exhibited significant improvements compared to the PBS group. Four out of ten mice achieved a complete immune response to EO771 cancer, resulting in a remarkable reduction in tumor burden and notable delays in tumor growth (Fig. 4 *Q* and *R*). The 5G12-treated group demonstrated a 60% survival rate, whereas the PBS group had a 0% survival rate at the endpoint of the in vivo experiment (Fig. 4*S*). Treatment with the 5G12 antibodies was well tolerated, as no evident signs of toxicity were observed, and there were no differences in body weight among the various treatment groups (Fig. 4*T*). Furthermore, we tested the EMT-6 model, a BALB/c triple-negative (ER, PR, and HER2 negative) murine cell line with an invasive phenotype. EMT-6 has recently emerged as a valuable pre-clinical model for immune-oncology studies of triple-negative breast cancer. While complete removal of EMT-6 tumors was not achieved with 5G12 treatment, there was a significant reduction in tumor burden and tumor growth (*SI Appendix*, Figs. S19–S21).

Having demonstrated the efficacy of anti-Siglec-15 in inhibiting bone metastasis growth in murine models, we investigated whether the therapeutic impact of Siglec-15 blockade is dependent on T cells or osteoclasts. To deplete T cells, we initially treated the mice with anti-CD4 and anti-CD8 antibodies before inoculating them with 1×10^4 4T1 cells per mouse (51). As shown in *SI Appendix*, Fig. S22, we observed significant differences in the efficacy of 5G12 in mice with and without T cells, underscoring the crucial role of T cells in Siglec-15 blockade. Osteoclast depletion was carried out as previously reported, involving the administration of clodronate liposomes to the mice (52–54). Post-osteoclast depletion and bone tumor inoculation, we found no significant difference in the presence or absence of anti-Siglec-15 treatment, highlighting the essential contribution of macrophages to the effectiveness of Siglec-15 blockade (*SI Appendix*, Fig. S22). Collectively, these data suggest that blocking Siglec-15 with 5G12 effectively decreases tumor burden and tumor growth in breast cancer bone metastasis.

Blocking Siglec-15 Inhibited Metastasis-to-Metastasis from Bone Lesions. Recent studies have indicated that established bone lesions in breast cancer patients can give rise to multi-organ metastases in the late stage of the disease, significantly reducing the survival rate (Fig. 5*A*) (8, 55, 56). Next, we investigated

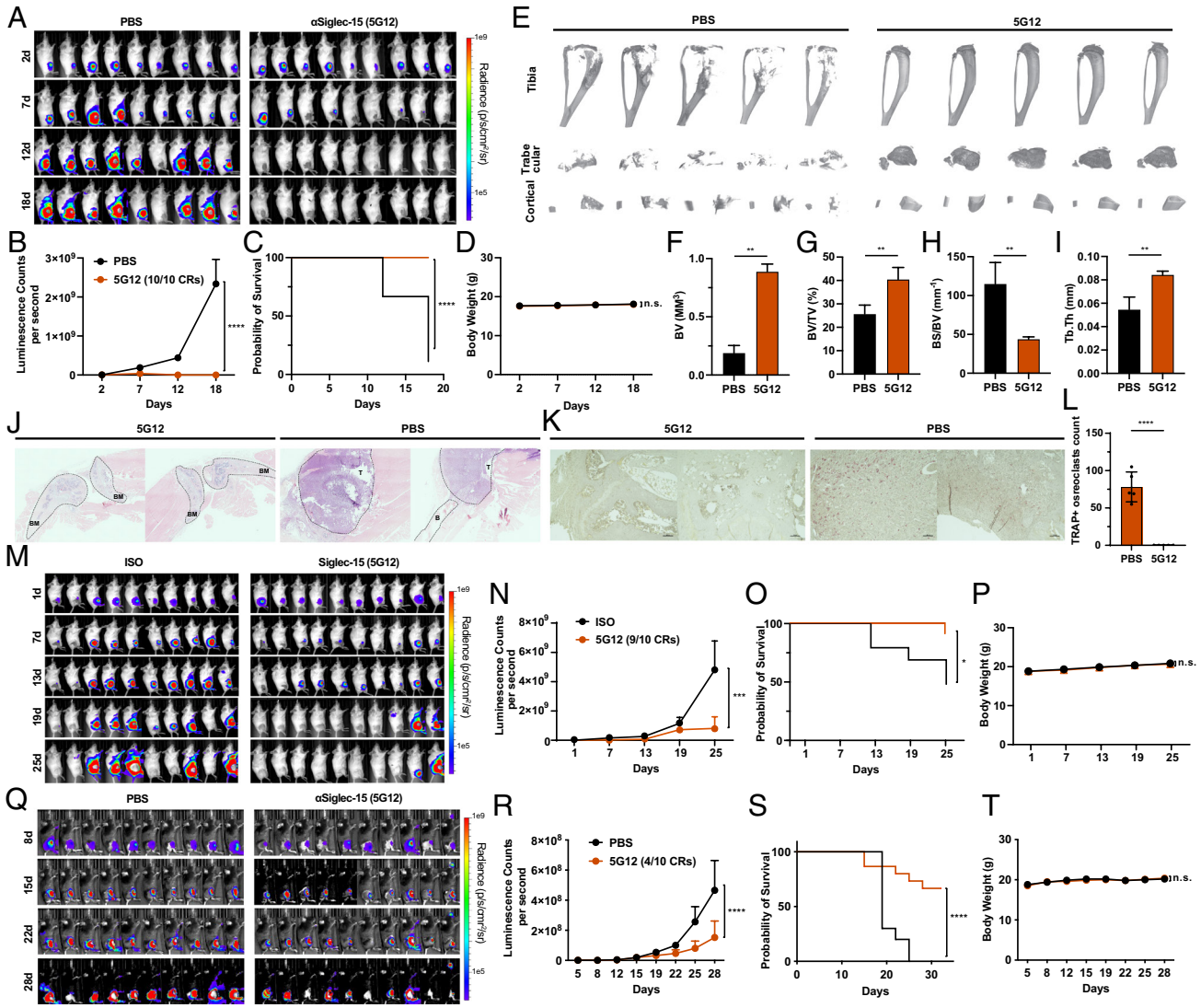

Fig. 4. Anti-Siglec-15 inhibits bone metastasis. (*A*) 4T1-luc2 cells were para-tibia injected into the right hind limb and treated by PBS and 5G12 as described in *Methods*. Tumor burden was monitored by weekly bioluminescence imaging. (*B*) Tumor growth curve measured by bioluminescence intensity and quantified by the IVIS® system. Data are mean ± S.E.M. (n = 9 mice per group). P values by two-way ANOVA. (*C*) Kaplan−Meier plot of the time-to-euthanasia of mice treated as described in (*A*). (*D*) Body weight change of tumor-bearing mice over time. (*E*) Micro-CT scanning of the tibia from mice in (*A*), trabecular bone and cortical bone were reconstructed by using NRecon software. (*F–I*) Quantitative analysis of bone volume (BV), bone volume/tissue volume ratio (BV/TV), bone surface/bone volume ratio (BS/BV), and trabecular thickness (Tb.Th). n = 5 independent experiments. The P value was calculated by the paired t-test. (*J*) Representative longitudinal, midsagittal hematoxylin and eosin (H&E)–stained sections of the tibia/femur from each group. T, tumor; B, bone; BM, bone marrow. (*K*) Representative images of TRAP staining of bone sections from each group. (*L*) Osteoclast number per image calculated at the tumor-bone interface in each group [red cells in (*K*) were considered as osteoclast positive cells]. (*M*) 4T1-luc2 cells were para-tibia injected into the right hind limb and treated by human isotope IgG1 (Iso) and 5G12 as described in *Methods*. Tumor burden was monitored by weekly bioluminescence imaging. (*N*) Tumor growth curve measured by bioluminescence intensity and quantified by IVIS® system. Data are mean ± S.E.M. (n = 9 mice per group). P values by two-way ANOVA. (*O*) Kaplan−Meier plot of the time-to-euthanasia of mice treated as described in (*M*). (*P*) Body weight change of tumor-bearing mice over time. (*Q*) EO771-GFP/luciferase cells were para-tibia injected into the right hind limb and treated by PBS and 5G12 as described in *Methods*. Tumor burden was monitored by weekly bioluminescence imaging. (*R*) Tumor growth curve measured by bioluminescence intensity and quantified by IVIS® system. Data are mean ± S.E.M. (n = 10 mice per group). P values by two-way ANOVA. (*S*) Kaplan−Meier plot of the time-to-euthanasia of mice treated as described in (*Q*). (*T*) Body weight change of tumor-bearing mice over time. $P > 0.05$ [not significant (n.s.)], $^{*}P < 0.05$, $^{**}P < 0.01$, $^{***}P < 0.001$, and $^{****}P < 0.0001$.

whether blocking Siglec-15 could impede the development of these secondary metastases originating from bone lesions. To examine this, we injected 5×10^3 4T1 cells labeled with firefly luciferase into the right hind limb of BALB/c mice through para-tibial injection, followed by treatment with 5G12 and PBS. In this model, localized tumors developed primarily in the tibiae at an early stage. However, as the bone lesions progressed, metastases marked by bioluminescence signals began to disseminate to other major organs, including the lungs, liver, spleen, kidneys, brain, and skeleton. At the endpoint, these organs were dissected to assess metastasis. As shown in Fig. 5 *B–D*, 77% of mice in the control group developed multi-organ metastases, with the lungs being the most affected organ, as all mice with secondary metastases showed lung involvement. Additionally, three mice in the control group developed skeletal metastases, suggesting that the skeletal system is also affected by late-stage bone lesions. Encouragingly, no secondary metastatic tumors were detected in the 5G12 treatment group, indicating that blocking Siglec-15 inhibits further dissemination of bone metastases effectively. A similar trend was observed in the EO771 model. We injected 1×10^5 EO771 cells labeled with firefly luciferase and GFP into the right hind limb of C57BL/6 J mice through para-tibial injection, followed by treatment with 5G12 and PBS. The results showed that 80% of mice in the control group developed multi-organ

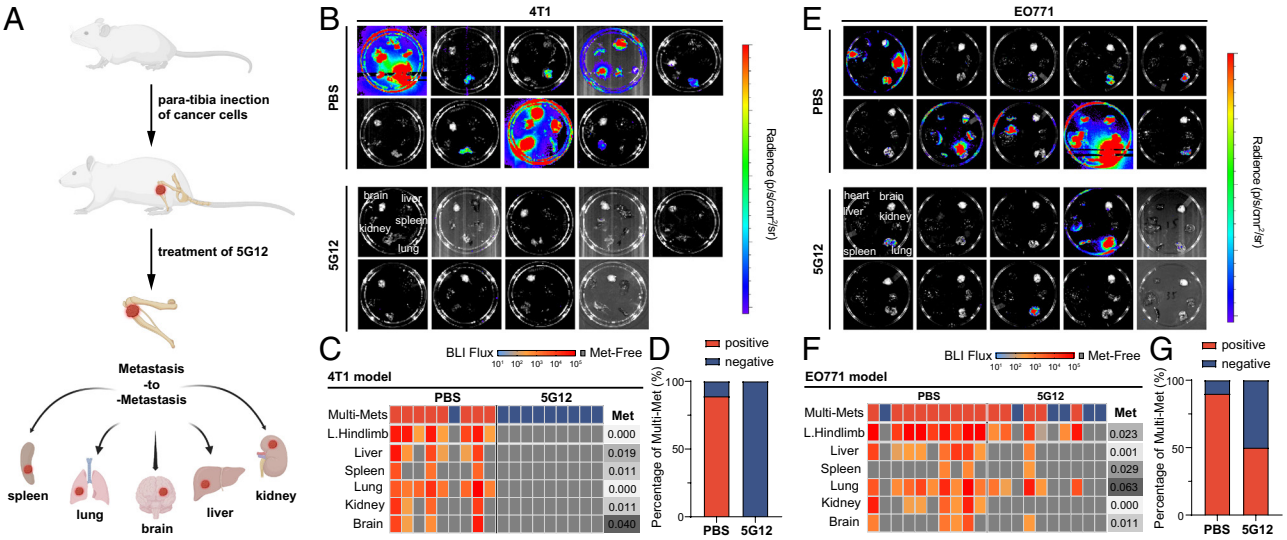

Fig. 5. Siglec-15 blockage prevents secondary metastases from bone lesions. (*A*) Bone lesions more readily give rise to secondary metastases to multiple organs. (*B*) Secondary metastases of PBS-treated (*Top*, *n* = 9) and 5G12-treated (*Bottom*, *n* = 9) 4T1 bone tumors were detected by bioluminescence imaging after dissection. (*C*) Heat map of ex vivo BLI intensity and status of metastatic involvement in tissues from the 4T1 tumor model mice treated with PBS and 5G12. Each column represents an individual animal, and each row represents a type of tissue. The presence of metastasis was defined as the presence of BLI signal above 30 counts/pixel under 60 s exposure time. Multisite metastases were defined as the metastatic involvement of at least two tissues. *P*-values were determined by Fisher's exact test on the frequency of metastatic involvement while by the Mann−Whitney test of the metastatic burden. (*D*) The ratio of multi-site metastasis of 4T1 tumor model mice. (*E*) Secondary metastases of PBS-treated (*Top*, *n* = 10) and 5G12-treated (*Bottom*, *n* = 10) EO771 bone tumors were detected by bioluminescence imaging after dissection. (*F*) Heat map of ex vivo BLI intensity and status of metastatic involvement in tissues from EO771 tumor model mice treated with PBS and 5G12 as described in (*C*). (*G*) The ratio of multi-site metastasis of EO771 tumor model mice.

metastases, with the lungs and liver being the most affected organs (Fig. 5 *E*–*G*). In contrast, the 5G12 treatment group exhibited a significantly reduced incidence of secondary metastases, while 6 of 10 mice carried bone metastases, only one developing multi-organ metastases. Among the mice with secondary metastases in the 5G12 group, 80% exclusively exhibited lung metastases. Notably, one mouse in the 5G12 treatment group had a relatively late-stage primary tumor but did not develop any secondary metastasis. These data suggest that blocking Siglec-15 in osteolytic bone metastatic niches can inhibit the growth of bone metastasis and prevent secondary metastases originating from bone lesions.

Discussion

Despite a high 5-y survival rate of over 90%, a substantial portion (20 to 40%) of breast cancer survivors will eventually experience metastases to distant organs, even years after undergoing surgeries (57). Among these metastases, bone is the most common site, accounting for over 47% of first-site metastases, followed by the lung, liver, and brain (1). The prognosis for breast cancer patients with bone metastases is challenging, with a 1-y survival rate of 51% and a 5-y survival rate dropping to 13% (5, 58). Consequently, there is a pressing need for therapies that can improve outcomes for breast cancer patients with bone metastases. While immunotherapy has emerged as a promising approach for metastatic breast cancer (MBC) treatment, its efficacy in patients with bone metastases has been disappointing. Immune checkpoint inhibitors (ICIs) have shown effectiveness in several cancer types (59–61), but their success in breast cancer has been limited, particularly in breast cancer patients with bone metastases. For instance, a phase III clinical trial evaluating atezolizumab for metastatic triple-negative breast cancer demonstrated that progression-free survival was significantly longer in the atezolizumab group compared to the placebo group. However, among breast cancer patients with bone metastases, there was no significant difference in the risk of progression or death between the atezolizumab and placebo groups (median progression-free survival: 5.7 vs. 5.2 mo; stratified hazard ratio for progression or death: 1.02; 95% CI: 0.79–1.31) (12). These findings suggest that the current immunotherapy approaches have limited efficacy when it comes to bone tumors.

The glycocalyx, a network of glycolipids and glycoproteins on cell surfaces, plays a pivotal role in immune modulation and is exploited by tumors to evade immune recognition. One prominent tumor glycosignature is hypersialylation. The identification of a large family of Siglec receptors has accelerated the understanding of sialic acid–binding immunoreceptors. Siglec-15, a member of the Siglec family proteins, is normally expressed on a subset of myeloid cells but becomes upregulated on tumor-infiltrating myeloid/macrophage cells, leading to suppression of antigen-specific T cell responses. In this study, we observed upregulation of Siglec-15 in both macrophages and osteoclasts within the bone metastatic niches of human and mouse samples. This upregulation contributes to the establishment of an immunosuppressive microenvironment. Siglec-15 upregulation on osteoclasts promotes tumor cell-mediated osteoclastogenesis while inhibiting T cell activity, facilitating the growth of bone cancer and further secondary metastases. Treatment with anti-Siglec-15 antibody demonstrated high efficacy in various syngeneic breast tumor models, resulting in T cell activation and proliferation, which gives a remarkable response rate. Furthermore, blocking Siglec-15 in osteolytic bone metastatic niches effectively inhibits the growth of bone metastases and prevents secondary metastases originating from bone lesions. While the therapeutic efficacy of Siglec-15 blockade has been remarkable, our understanding of the molecular mechanism underlying the Siglec-15/sialic acid axis remains limited. Previous research has hinted at CD44 being a potential ligand on osteoclasts (62), and a more recent investigation has proposed CD11b as a ligand on T cells (63). These findings imply that Siglec-15 may have the capacity to bind to multiple ligands depending on the cell type, underscoring the need for more rigorous studies to identify its ligands on various cell types. Nevertheless, further research is essential to validate these biochemical mechanisms.

The Siglec-15/sialic acid axis represents as a glycoimmune checkpoint and modulator of tumor-induced osteoclastogenesis for bone cancers. Targeting this Siglec-15/sialic acid axis in the bone could be beneficial for patients with bone cancers and bone metastases from other primary cancer types, as the bone is a preferential site for metastasis in prostate, lung, kidney, and thyroid cancers.

Methods

Human Bone Metastasis Samples. The protocols for collecting and utilizing human bone metastasis samples were conducted in compliance with the principles outlined in the Declaration of Helsinki. These protocols were approved by the Institutional Review Boards at Baylor College of Medicine (H-49396), the University of Texas MD Anderson Cancer Center (PA15-0225), and the University of Texas Medical Branch (H-46675). Prior to undergoing orthopedic surgery, all patients provided written informed consent for the use of their samples in research endeavors.

Bone Sectioning. The bone tissues were fixed in 4% paraformaldehyde at 4 °C for 24 h. Following fixation, the tissues were washed with PBS and subsequently subjected to 14% EDTA for decalcification. Decalcification was carried out for 5 d (bone fragments) or up to 2 wk (intact bones). The Breast Center Pathology Core at Baylor College of Medicine will assist to perform the paraffin embedding and microtome sectioning (4 μm) for bone fragments and perform OCT embedding and frozen sectioning (10 μm) for the intact bones.

Immunofluorescent Staining on Bone Sections. For paraffin-embedded sections, slides were baked at 55 °C for 2 h, dewaxed, and rehydrated according to the standard protocol. Make antigen retrieval dilutions (PH 9.0) by mixing one part of 10X IHC Antigen Retrieval Solution (ThermoFisher, 00-4956-58) with nine parts of deionized water. The slides were immersed in the antigen retrieval dilutions and placed into a pressure cooker. The pressure cooker was set at 125 °C and 25 psi for 10 min. After the antigen retrieval process, the slides were allowed to cool down to room temperature. For frozen sections, the slides were thawed at room temperature for 10 min. Following the thawing process, the slides were incubated in PBS (phosphate-buffered saline) for an additional 10 min. All the slides underwent treatment with a 0.1 M NH_4Cl solution for a duration of 10 min to reduce autofluorescence. Following this, they were blocked using a 10% donkey serum solution in PBS-GT (2% Gelatin, 0.5% TritonX-100) for 1 h at room temperature. The slides were then incubated with the specific primary antibodies at 4 °C for overnight and then stained with corresponding secondary antibodies at room temperature for 1 h. The primary antibodies used in this study were Rabbit anti-CTSK (Abcam, ab19027), Rabbit anti-CD8 (Abcam, ab217344), Rat anti-CD4 (ThermoFisher, 14-9766-82), Chicken anti-GFP (Novus Biologicals, NB100-1614), Rabbit anti-Siglec15 (Invitrogen, PA5-72765), Rat anti-F4/80 (Cell Signaling Technology, 71299), Pan Cytokeratin Monoclonal Antibody-Alexa Fluor™ 488 (Invitrogen, 53-9003-82), and 5G12.

Osteoclastogenesis Assay, qPCR, and TRAP Staining. RAW264.7 cells were purchased from American Type Culture Collection and cultured according to the American Type Culture Collection instructions. To induce osteoclastogenesis, RAW264.7 was seeded in a 24-well plate at a density of 1×10^4 cells/well and allowed to adhere overnight. The medium was replaced, and the cells were treated with 50 ng/mL RANKL from R&D system (462-TEC-010/CF) for 4 d. For co-culture experiments with tumor cells, RAW264.7 cells were seeded at 3×10^4 cells/well on day 1 and allowed to adhere overnight. MDA-MB-231 and E0771 cells were seeded at 1×10^4 cells/well were added to the RAW264.7-containing wells on day 2, and co-cultured for 4 d before TRAP staining. TRAP staining was performed using Leukocyte Acid Phosphatase (TRAP) Kit (Sigma-Aldrich, 387A) following the provided procedure. The cells for qPCR study were prepared as described as above; an extra group was treated with 10 μg/mL of 5G12. The expression level of mRNA was analyzed by RT-qPCR at day 4. Primers can be found in *SI Appendix*.

Detection of Cytokine Release. RAW264.7 cell was seeded in a 24-well plate at a density of 1×10^4 cells/well and allowed to adhere overnight. RAW264.7 cell was divided into three groups: 1) no treatment, as pre-osteoclast; 2) osteoclast, treated with 50 ng/mL RANKL; and 3) 5G12 treatment, treatment with 50 ng/mL RANKL and 10 μg/ml 5G12 antibody. Three groups were cultured for 4 d, the supernatants were collected on day 4, at the time of collection, no significant difference in cell number was observed. IL-6 and TNF-α levels were detected by ELISA (Biolegend, 431307 and 430907). The experiment followed the instructions provided by the kits.

BICA. The BICA experiment was performed as previously reported (49). The tumor-free bone fragments were obtained and arranged in a low-attachment 96-well plate. Then, 5,000 E0771 cells were added to each well and cultured in a 37 °C incubator for 24 h. Following incubation, the wells were thoroughly washed and rinsed with PBS to completely eliminate any unattached cancer cells. The bioluminescence intensities of all the cancer cells present in the bone were measured using the IVIS Lumina II system (PerkinElmer, Advanced Molecular Vision) as the baseline (day 0). After the imaging process, the culture medium was replenished, and the antibody was introduced at different concentrations. Subsequently, all the bioluminescence data were analyzed using the Living Image Software (PerkinElmer, v4.7.3) and normalized with the day 0 data.

CD8+ OT-1 T Cell Isolation and Activation. The spleen cells of OT-1 mice were dissociated by mechanical disruption and lysed in the red blood cells (RBC) lysis buffer (Tonbo Biosciences, TNB-4300-L100). For sorting CD8+ T cells, spleen cells were stained with Biotin anti-B220, Biotin anti-CD11b, Biotin anti-Gr1, Biotin anti-Ter119 (all from BD Pharmingen™ Biotin Mouse Lineage Panel, 559971), Biotin anti-CD11c (Tonbo, 30-0114), and Biotin anti-CD4(Tonbo, 30-0041), followed by incubating with Streptavidin Particles (BD IMag™ Streptavidin Particles Plus, 557812) for 15 min. After incubation, CD8+ T cells (Biotin-) were collected in the remaining supernatant, while non-CD8+ T cells (Biotin+) were enriched and separated by using magnet negative selection (STEMCELL, EasySep™ Cell Separation magnet, #18000). After isolation of CD8+ OT-1 T cells, they were cultured in a T cell culture medium, which consisted of RPMI-1640 medium (HyClone) supplemented with 10% heat-inactivated fetal bovine serum (FBS) that was heat-inactivated at 56 °C for 30 min, HEPES (5 mM), Glutamax (2 mM), Penicillin/Streptomycin (50 mg/mL), non-essential amino acids (NEAA, 5 mM), sodium pyruvate (5 mM), beta-mercaptoethanol (50 μM) and human IL-2 (20 ng/mL). To activate the T cells, they were incubated with a 1:1 ratio of CD3/CD28 Dynabeads for a period of 48 h. After activation, T cells were separated from Dynabeads using EasySep magnet, allowing for the isolation of the activated T cells for further experiment.

In Vitro Co-culture Assay. For co-culture of osteoclasts and CD8+ OT-1 T cells, bone marrow from WT mice was flushed and lysed in RBC lysis buffer. After isolation of bone marrow cells, they are cultured in an Osteoclast differentiation (OCD) medium, which consisted of MEM Alpha Modification medium (HyClone) supplemented with 25 ng/mL Recombinant Murine M-CSF(PeproTech, 315-02) and 60 ng/mL Recombinant Murine sRANK Ligand (PeproTech, 315-11) for 7 d. The medium was replenished with fresh OCD medium every 48 h. The differentiated osteoclasts were co-cultured with CD3/CD28 activated T cells at a 1:5 ratio for 48 h. 5G12 (anti-Siglec15) was added when co-culture started. For the T cell cytotoxicity assay, the differentiated osteoclasts were co-cultured with CD3/CD28 activated T cells at a 1:1 ratio. Additionally, 5G12 was added to the co-culture at the start. After 48 h of co-culture, the cells were mixed in a 1:1:5 ratio with E0771-OVA cells and further incubated for an additional 2 d. Following this, the cells were collected and analyzed using flow cytometry. Flow antibody used in the study were CD45-VF450 (Tonbo, 75-0459), CD8-BV711 (BioLegend, 100747), CD3e-PerCP/Cy5.5 (Tonbo, 65-0031), PD-1-PE (Tonbo, 50-9985), TIM-3-APC (Tonbo, 20-5870), and LAG3-PE (Tonbo, 50-2231). Prior to flow cytometry analysis, the cells were resuspended in PBS containing 2% FBS. To aid in cell viability and nuclear staining, DAPI (Invitrogen™ R37606) was added to the PBS solution. Additionally, liquid counting beads from BD Bioscience (335925) were included for accurate cell counting during the analysis. All flow cytometry analyses were conducted using a BD LSRFortessa instrument, and the resulting data were analyzed using FlowJo software.

Animal Models. Para-tibia injections and in vivo imaging system (IVIS) imaging were performed. For the E0771 model, 1×10^5 E0771-GFP/FLuc cells were inoculated into the right hind limb tibia of 7–8 weeks female C57BL/6J mice at day 0, 5 d after injection, the animals were randomized into two groups: PBS-treated control and 5G12 treatment. The first treatment was given on day 5, 200 μg/mice, i.p. The treatment was repeated twice per week for 3 wk,

six doses in total were given. The animals were imaged twice a week using IVIS Lumina II (Advanced Molecular Vision), following the recommended procedures and manufacturer's settings. On day 28, mice were anesthetized and blood was collected by cardiac puncture before euthanasia. The liver, spleen, lung, brain, kidney, and skeleton were collected for further tests. For the 4T1 model, 1×10^4 4T1-luc2 cells (ATCC, CRL-2539-LUC2™) were inoculated intothe right hind limb tibia of 7–8 weeks female BALB/c at day 0; 2 d after injection, the animals were randomized into two groups: PBS-treated control and 5G12 treatment. The first treatment was given on day 2, 200 μg/mice, i.p. The treatment was repeated three times, given at day 2, day 6, and day 10. For the isotype control experiment, the 4T1 tumor was inoculated as described above, the animals were randomized into two groups: isotype control and 5G12 treatment. human IgG1 isotype (BioXCell, BE0297) was used as an isotype control antibody, the treatment was repeated three times, given at day 2, day 7, and day 13, 200 μg/mice, i.p. Same ex vivo study was applied to this model as described above. For the EMT-6 model, 1×10^5 EMT-6-FLuc cells were inoculated into the right hind limb tibia of 7–8 weeks female BALB/c mice at day 0; 1 d after injection, the animals were randomized into two groups: PBS-treated control and 5G12 treatment. The first treatment was given on day 1, 200 μg/mice, i.p. The treatment was repeated twice per week for 3 wk, six doses in total were given. For osteoclast (macrophages) depletion study, clodronate liposome (C-010, Liposoma BV) was injected intraperitoneally at 4-d intervals from 6 d before tumor inoculation and repeated for four times at a dose of 0.3 mL of liposomes as reported previously (52–54). In addition, 1×10^4 4T1-luc2 cells were inoculated into the tibia at day 0. The experiment group was treated with 5G12 antibody intraperitoneally at day 2 and day 6, 200 μg/mice. For T cell depletion study, mice were treated with intraperitoneal injection of an initial dose of 200 μg/mouse of anti-CD4 (clone GK1.5, BioXCell) and anti-CD8 (clone 2.43, BioXCell) antibodies, followed by similar dosing with 150 μg/mouse every 4 d for three times (51). In addition, 1×10^4 4T1-luc2 cells were inoculated into the tibia at day 0. The mice were treated with 5G12 antibody intraperitoneally at day 2 and day 6, 200 μg/mice.

All experimental procedures were approved by the Institutional Animal Care and Use Committee at Rice University.

Ex Vivo Metastasis-to-Metastasis Analysis. Mice were anesthetized with 2.5% isoflurane in oxygen and injected with luciferin retro-orbitally. Mice were then euthanized, and their livers, spleens, lungs, kidneys, brain, and skeleton were collected. Ex vivo bioluminescence and fluorescence imaging of these organs were immediately performed on the IVIS Lumina.

Radiographic Analysis. Tibiae were dissected, fixed, and scanned by microCT (SkyScan 1272) at a resolution of 17.2 um per pixel. Raw images were reconstructed in NRecon and analyzed in CTAn (SkyScan) using a region of interest. Bone parameters analyzed included trabecular thickness (Tb.Th), bone volume fraction (BV/TV), and bone surface/bone volume ratio.

Data, Materials, and Software Availability. All study data are included in the article and/or *SI Appendix*.

ACKNOWLEDGMENTS. We thank Dr. Xiao Laboratory members for insightful comments. This work was supported by the Cancer Prevention Research Institute of Texas (CPRIT RR170014 to H.X.), NIH (R01-CA277838, R35-GM133706, R21-CA255894, and R01-AI165079 to H.X.), the Robert A. Welch Foundation (C-1970 to H.X.), US Department of Defense (HT9425-23-1-0494 and W81XWH-21-1-0789 to H.X.), the John S. Dunn Foundation Collaborative Research Award (to H.X.), and the Hamill Innovation Award (to H.X.). H.X. is a Cancer Prevention & Research Institute of Texas (CPRIT) scholar in cancer research.

Author affiliations: [a]Department of Chemistry, Rice University, Houston, TX 77005; [b]Department of Molecular and Cellular Biology, Baylor College of Medicine, Houston, TX 77030; [c]Department of Biosciences, Rice University, Houston, TX 77005; and [d]Department of Bioengineering, Rice University, Houston, TX 77005

1. R. E. Coleman, R. D. Rubens, The clinical course of bone metastases from breast cancer. *Br. J. Cancer* **55**, 61–66 (1987).
2. Y. S. DeRose *et al.*, Tumor grafts derived from women with breast cancer authentically reflect tumor pathology, growth, metastasis and disease outcomes. *Nat. Med.* **17**, 1514–1520 (2011).
3. Y. Chen *et al.*, RANKL blockade prevents and treats aggressive osteosarcomas. *Sci. Transl. Med.* **7**, 317ra197 (2015).
4. C. M. Rutter *et al.*, Secular trends in colon and rectal cancer relative survival. *J. Natl. Cancer Inst.* **105**, 1806–1813 (2013).
5. E. Svensson, C. F. Christiansen, S. P. Ulrichsen, M. R. Rørth, H. T. Sørensen, Survival after bone metastasis by primary cancer type: A Danish population-based cohort study. *BMJ Open* **7**, e016022 (2017).
6. I. Adjei, M. Temples, S. Brown, B. Sharma, Targeted nanomedicine to treat bone metastasis. *Pharmaceutics* **10**, 205 (2018).
7. R. E. Coleman, P. Smith, R. D. Rubens, Clinical course and prognostic factors following bone recurrence from breast cancer. *Br. J. Cancer* **77**, 336–340 (1998).
8. W. Zhang *et al.*, The bone microenvironment invigorates metastatic seeds for further dissemination. *Cell* **184**, 2471–2486.e20 (2021).
9. I. L. Bado *et al.*, The bone microenvironment increases phenotypic plasticity of ER+ breast cancer cells. *Dev. Cell* **56**, 1100–1117.e9 (2021).
10. L. Cheng, Y. Wang, Y. Guo, S. S. Zhang, H. Xiao, Advancing protein therapeutics through proximity-induced chemistry. *Cell Chem. Biol.* (2023), 10.1016/j.chembiol.2023.09.004.
11. G. Morad, B. A. Helmink, P. Sharma, J. A. Wargo, Hallmarks of response, resistance, and toxicity to immune checkpoint blockade. *Cell* **184**, 5309–5337 (2021).
12. P. Schmid *et al.*, Atezolizumab and Nab-paclitaxel in advanced triple-negative breast cancer. *N. Engl. J. Med.* **379**, 2108–2121 (2018).
13. J. Lübbers, E. Rodríguez, Y. van Kooyk, Modulation of immune tolerance via Siglec-Sialic acid interactions. *Front. Immunol.* **9**, 2807 (2018).
14. S. Pillai, I. A. Netravali, A. Cariappa, H. Mattoo, Siglecs and immune regulation. *Annu. Rev. Immunol.* **30**, 357–392 (2012).
15. P. R. Crocker, J. C. Paulson, A. Varki, Siglecs and their roles in the immune system. *Nat. Rev. Immunol.* **7**, 255–266 (2007).
16. P. R. Crocker, A. Varki, Siglecs, sialic acids and innate immunity. *Trends Immunol.* **22**, 337–342 (2001).
17. M. S. Macauley, P. R. Crocker, J. C. Paulson, Siglec-mediated regulation of immune cell function in disease. *Nat. Rev. Immunol.* **14**, 653–666 (2014).
18. Z. Fehervari, Targeting cancer by Siglecs. *Nat. Immunol.* **19**, 1148 (2018).
19. T. Angata, C. M. Nycholat, M. S. Macauley, Therapeutic targeting of Siglecs using antibody- and glycan-based approaches. *Trends Pharmacol. Sci.* **36**, 645–660 (2015).
20. S. Hong *et al.*, Glycoengineering of NK cells with glycan ligands of CD22 and selectins for B-cell lymphoma therapy. *Angew. Chem. Int. Ed.* **60**, 3603–3610 (2021).
21. D. Sgroi, A. Varki, S. Braesch-Andersen, I. Stamenkovic, CD22, a B cell-specific immunoglobulin superfamily member, is a sialic acid-binding lectin. *J. Biol. Chem.* **268**, 7011–7018 (1993).
22. G. M. Doody *et al.*, A role in B cell activation for CD22 and the protein tyrosine phosphatase SHP. *Science* **269**, 242–244 (1995).
23. B. E. Collins, B. A. Smith, P. Bengtson, J. C. Paulson, Ablation of CD22 in ligand-deficient mice restores B cell receptor signaling. *Nat. Immunol.* **7**, 199–206 (2006).
24. J. Müller *et al.*, CD22 ligand-binding and signaling domains reciprocally regulate B-cell Ca^{2+} signaling. *Proc. Natl. Acad. Sci. U.S.A.* **110**, 12402–12407 (2013).
25. S. Han, B. E. Collins, P. Bengtson, J. C. Paulson, Homomultimeric complexes of CD22 in B cells revealed by protein-glycan cross-linking. *Nat. Chem. Biol.* **1**, 93–97 (2005).
26. J. Ereño-Orbea *et al.*, Molecular basis of human CD22 function and therapeutic targeting. *Nat. Commun.* **8**, 764 (2017).
27. M. K. O'Reilly, H. Tian, J. C. Paulson, CD22 is a recycling receptor that can shuttle cargo between the cell surface and endosomal compartments of B cells. *J. Immunol.* **186**, 1554–1563 (2011).
28. M. S. Macauley *et al.*, Antigenic liposomes displaying CD22 ligands induce antigen-specific B cell apoptosis. *J. Clin. Invest.* **123**, 3074–3083 (2013).
29. C. D. Rillahan *et al.*, Disubstituted Sialic acid ligands targeting Siglecs CD33 and CD22 associated with myeloid leukaemias and B cell lymphomas. *Chem. Sci.* **5**, 2398–2406 (2014).
30. H. Choi *et al.*, Development of Siglec-9 blocking antibody to enhance anti-tumor immunity. *Front. Oncol.* **11**, 778989 (2021).
31. M. Islam *et al.*, Suppressing immune responses using Siglec ligand-decorated anti-receptor antibodies. *J. Am. Chem. Soc.* **144**, 9302–9311 (2022).
32. M. Boyce *et al.*, Metabolic cross-talk allows labeling of O-linked β-*N*-acetylglucosamine-modified proteins via the *N*-acetylgalactosamine salvage pathway. *Proc. Natl. Acad. Sci. U.S.A.* **108**, 3141–3146 (2011).
33. L. J. Edgar *et al.*, Sialic acid ligands of CD28 suppress costimulation of T cells. *ACS Cent. Sci.* **7**, 1508–1515 (2021).
34. H. Xiao, E. C. Woods, P. Vukojicic, C. R. Bertozzi, Precision glycocalyx editing as a strategy for cancer immunotherapy. *Proc. Natl. Acad. Sci. U.S.A.* **113**, 10304–10309 (2016).
35. M. Gray *et al.*, Targeted desialylation overcomes glyco-immune checkpoints and potentiates the anticancer immune response in vivo. *Nat. Chem. Biol.* **16**, 1376–1384 (2020), 10.26434/chemrxiv.8187146.v2.
36. Q. Li *et al.*, Integrative analysis of Siglec-15 mRNA in human cancers based on data mining. *J. Cancer* **11**, 2453–2464 (2020).
37. B. Li *et al.*, Expression signature, prognosis value, and immune characteristics of Siglec-15 identified by pan-cancer analysis. *Oncoimmunology* **9**, 1807291 (2020).
38. J. Wang *et al.*, Siglec-15 as an immune suppressor and potential target for normalization cancer immunotherapy. *Nat. Med.* **25**, 656–666 (2019), 10.1038/s41591-019-0374-x.
39. G. Murugesan *et al.*, Siglec-15 recognition of Sialoglycans on tumor cell lines can occur independently of Sialyl Tn antigen expression. *Glycobiology* **31**, 44–54 (2020), 10.1093/glycob/cwaa048.
40. J. Sun, Q. Lu, M. F. Sanmamed, J. Wang, Siglec-15 as an emerging target for next-generation cancer immunotherapy. *Clin. Cancer Res.* **27**, 680–688 (2021).
41. K.-H. Lim, Y. Yang, L. M. Staudt, Pathogenetic importance and therapeutic implications of NF-κB in lymphoid malignancies: NF-κB in lymphoid cancer. *Immunol. Rev.* **246**, 359–378 (2012).
42. R. B. Parker, J. J. Kohler, Regulation of intracellular signaling by extracellular glycan remodeling. *ACS Chem. Biol.* **5**, 35–46 (2010).

43. Y. Kameda *et al.*, Siglec-15 regulates osteoclast differentiation by modulating RANKL-induced phosphatidylinositol 3-Kinase/Akt and Erk pathways in association with signaling adaptor DAP12. *J. Bone Miner. Res.* **28**, 2463–2475 (2013).
44. N. Ishida-Kitagawa *et al.*, Siglec-15 protein regulates formation of functional osteoclasts in concert with DNAX-activating protein of 12 kDa (DAP12). *J. Biol. Chem.* **287**, 17493–17502 (2012).
45. Y. Hiruma, T. Hirai, E. Tsuda, Siglec-15, a member of the sialic acid-binding lectin, is a novel regulator for osteoclast differentiation. *Biochem. Biophys. Res. Commun.* **409**, 424–429 (2011).
46. M. Stuible *et al.*, Mechanism and function of monoclonal antibodies targeting Siglec-15 for therapeutic inhibition of osteoclastic bone resorption. *J. Biol. Chem.* **289**, 6498–6512 (2014).
47. D. Sato *et al.*, Siglec-15-targeting therapy increases bone mass in rats without impairing skeletal growth. *Bone* **116**, 172–180 (2018).
48. R. Takamiya, K. Ohtsubo, S. Takamatsu, N. Taniguchi, T. Angata, The interaction between Siglec-15 and tumor-associated sialyl-Tn antigen enhances TGF- secretion from monocytes/macrophages through the DAP12-Syk pathway. *Glycobiology* **23**, 178–187 (2013).
49. Y.-H. Wu *et al.*, Optimization and characterization of a bone culture model to study prostate cancer bone metastasis. *Mol. Cancer Ther.* **21**, 1360–1368 (2022).
50. H. Wang *et al.*, Bone-in-culture array as a platform to model early-stage bone metastases and discover anti-metastasis therapies. *Nat. Commun.* **8**, 15045 (2017).
51. K. N. Balogh, D. J. Templeton, J. V. Cross, Macrophage migration inhibitory factor protects cancer cells from immunogenic cell death and impairs anti-tumor immune responses. *PLoS ONE* **13**, e0197702 (2018).
52. N. Van Rooijen, A. Sanders, T. K. Van Den Berg, Apoptosis of macrophages induced by liposome-mediated intracellular delivery of clodronate and propamidine. *J. Immunol. Methods* **193**, 93–99 (1996).
53. N. Van Rooijen, A. Sanders, Elimination, blocking, and activation of macrophages: Three of a kind? *J. Leukoc. Biol.* **62**, 702–709 (1997).
54. H. Lin, J. P. O'Connor, Osteoclast depletion with clodronate liposomes delays fracture healing in mice. *J. Orthop. Res.* **35**, 1699–1706 (2017).
55. H. Wang *et al.*, The osteogenic niche is a calcium reservoir of bone micrometastases and confers unexpected therapeutic vulnerability. *Cancer Cell* **34**, 823–839.e7 (2018).
56. M. Li *et al.*, A simple and cost-effective assay for measuring anti-drug antibody in human patients treated with Adalimumab. *J. Immunol. Methods* **452**, 6–11 (2018).
57. H. Kennecke *et al.*, Metastatic behavior of breast cancer subtypes. *J. Clin. Oncol.* **28**, 3271–3277 (2010).
58. A. Parkes *et al.*, Prognostic factors in patients with metastatic breast cancer with bone-only metastases. *Oncologist* **23**, 1282–1288 (2018).
59. P. Sharma, J. P. Allison, Immune checkpoint targeting in cancer therapy: Toward combination strategies with curative potential. *Cell* **161**, 205–214 (2015).
60. D. M. Pardoll, The blockade of immune checkpoints in cancer immunotherapy. *Nat. Rev. Cancer* **12**, 252–264 (2012).
61. L. Galluzzi, T. A. Chan, G. Kroemer, J. D. Wolchok, A. López-Soto, The hallmarks of successful anticancer immunotherapy. *Sci. Transl. Med.* **10**, eaat7807 (2018).
62. L. Chang *et al.*, Identification of Siglec ligands using a proximity labeling method. *J. Proteome Res.* **16**, 3929–3941 (2017).
63. M. P. Lenza *et al.*, Structural insights into Siglec-15 reveal glycosylation dependency for its interaction with T cells through integrin CD11b. *Nat. Commun.* **14**, 3496 (2023).